Soils and Foundations 2014;54(6):1081–1093

HOSTED BY

ELSEVIER

The Japanese Geotechnical Society

Soils and Foundations

www.sciencedirect.com
journal homepage: www.elsevier.com/locate/sandf

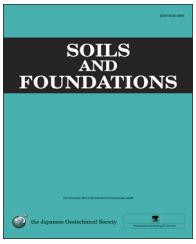

Shear banding in torsion shear tests on cross-anisotropic deposits of fine Nevada sand

Poul V. Lade[a,*], Eugene Van Dyck[b], Nina M. Rodriguez[c]

[a]Department of Civil Engineering, The Catholic University of America, Washington, DC 20064, USA
[b]Schnabel Services, Inc., Glen Allen, VA 23059, USA
[c]Department of the Navy, Naval Sea Systems Command 05C, Washington Navy Yard, Washington, DC 20376, USA

Received 21 March 2013; received in revised form 8 July 2014; accepted 14 August 2014
Available online 11 December 2014

Abstract

A series of torsion shear experiments was performed on large hollow cylinder specimens of Fine Nevada sand with major principal stress directions relative to vertical, α, varying from 0° to 90° and with the intermediate principal stress, σ_2, varying from σ_3 to σ_1 as indicated by $b=(\sigma_2-\sigma_3)/(\sigma_1-\sigma_3)$. The Fine Nevada sand was deposited by dry pluviation, thus producing a sand fabric with horizontal bedding planes and cross-anisotropic characteristics. The various stress conditions were achieved by varying the pressures inside and outside the hollow cylinder specimen relative to the shear stress and the vertical deviator stress according to a pre-calculated pattern. All stresses and all strains were determined from careful measurements so that analysis of the soil behavior could be made reliably. The soil behavior was determined for a pattern of combinations of α varying with increments of 22.5° from 0° to 90° and b varying with increments of 0.25 from 0.0 to 1.0. Thus, 25 test locations were established, but many tests were repeated to study the consistency of the results. The friction angles varied considerably with α and b, thus indicating the importance of the intermediate principal stress and the principal stress directions relative to the horizontal bedding planes. The observed shear bands essentially followed the expected directions, but due to the cross-anisotropy shear bands were also observed in the direction of the major principal stress in regions with high b-values. The strength variation was also influenced by the flexibility of the boundaries in these regions.

Keywords: Cross-anisotropy; Sand; shear banding; Shear strength; Three-dimensional strength; Torsion shear; True triaxial tests (IGC: D6)

1. Introduction

The effects of principal stress direction relative to the bedding planes and the effects of the relative magnitude of the intermediate principal stress on the direction of shear banding in cross-anisotropic sand deposits is of interest. Therefore, a series of torsion shear tests on large hollow cylinder specimens prepared by dry pluviation was performed. To study the variation in shear strength and in direction of shear banding for all directions of the major principal stress relative to vertical, α, and all relative values of the intermediate principal stress, as expressed by $b=(\sigma_2-\sigma_3)/(\sigma_1-\sigma_3)$, a systematic program consisting of 25 drained torsion shear tests was performed. Since several of these experiments were repeated to check for accuracy and scatter, a total of 44 torsion shear tests were performed on Fine Silica sand deposited by dry pluviation, which creates cross-anisotropic deposits similar to those found in-situ. Situations in which the

*Corresponding author.
E-mail addresses: Lade@cua.edu (P.V. Lade), EVanDyck@schnabel-eng.com (E. Van Dyck), nina.m.rodriguez1@navy.mil (N.M. Rodriguez).
Peer review under responsibility of The Japanese Geotechnical Society.

http://dx.doi.org/10.1016/j.sandf.2014.11.004
0038-0806/

influence of principal stress direction can be isolated, while other parameters are held constant can be created and studied in a torsion shear apparatus, in which both the direction and magnitude of principal stresses can be controlled. With these devices, which allow for creation of three different principal stresses, it is possible to apply continuous, controlled increments and/or rotations of principal stresses in the vertical plane of the hollow cylinder specimen. The tests performed in this experimental program had different, varying internal and external pressures and therefore, were able to cover constant intermediate principal stress ratios as expressed by b, and principal stress directions, as expressed by α.

2. Shear strength components in granular materials

The shear strength of granular materials derives from different components as identified earlier (Rowe, 1962; Bishop, 1966; Lee and Seed, 1967). Thus, the measured friction angle consists of contributions from basic sliding friction between particles, energy input to overcome dilation, energy for rearrangement of particles (remolding) at constant volume and energy for particle crushing. The basic friction angle is considered to be constant at all confining pressures. While the basic friction and the dilation effects can be measured and quantified, the effects of remolding and crushing are not quantifiable. It is however, possible to calculate them as the difference between the measured friction angle and the effects of dilation. In undrained tests remolding at constant volume results in an additional contribution to the shear strength above the basic friction effect. The crushing component is small at low confining pressures where dilation is important, while the effect of dilation vanishes at high confining pressures, where particle crushing is prevalent. Thus, particle crushing is dominant at high confining pressures and volume changes, which are so important for soil behavior at low confining pressures, are suppressed and the shear strength is caused by the crushing strength of sand particles. The resulting friction angle is constant at these high confining pressures and the shear strength is simply proportional to the confining pressure (Lade and Yamamuro, 1996, Yamamuro and Lade, 1996). While the friction angle for dense Cambria sand varied with confining pressure due to the contribution of dilation at lower confining pressures, it became constant at confining pressures higher than 15 to 20 MPa (Yamamuro and Lade, 1996). The friction angle at high pressures represents the intrinsic shear strength of the sand and does not involve any effects of dilation or remolding at constant volume.

These components of shear strength do not have directional values, except the dilation angle. Thus, all cross-anisotropy relates to the variation of the angle of dilation obtained for different directions. This in turn is dependent on the particle fabric or structure in the soil.

3. Previous studies of cross-anisotropy

Studies of cross-anisotropy as influenced by the sand fabric were initially performed in triaxial compression on specimens in which the sand was deposited with bedding planes inclined at different angles, α, to the vertical axis of the specimen from 0° to 90°. These studies (Oda 1972a, 1972b, 1981; Oda et al., 1978; Tatsuoka et al., 1986; Lade and Wasif, 1988) indicated that the maximum strength was mobilized when the major principal stress was applied perpendicular to the bedding planes with a transition to lower strengths observed when the major principal stress was aligned with the bedding planes. While these tests were all performed with b=0.0, cross-anisotropy has also been studied in true triaxial equipment to investigate the effects of $b > 0.0$ (e.g. Yamada and Ishihara, 1979; Haruyama, 1981; Ochiai and Lade, 1983; Lam and Tatsuoka, 1988; Abelev and Lade 2003, 2004; Lade and Abelev 2003, 2005). The accumulated evidence shows that under monotonic conditions, when loading and deposition directions coincide, and when no rotation of principal stresses occurs, then the initial anisotropic fabric largely controls the deformation process and the peak shear resistance, especially in sands with elongated particles. This fact has been utilized in testing programs to study the influence of inherent cross-anisotropy on the failure criterion for such soils. The results obtained by Ochiai and Lade (1983), as well as those obtained by Yamada and Ishihara (1979), clearly showed cross-anisotropic stress–strain behavior. The failure surfaces, on the other hand, indicated only minor effects and were less clearly influenced by cross-anisotropy.

Only few studies have been performed to find the influence of b and α on the friction angle of sands for various combinations of these two variables. This may be done in directional shear or in torsion shear equipment with different pressures applied inside and outside the hollow cylinder specimen. Limited and sporadic experimental results have been provided in this respect by Arthur and Menzies (1972), Arthur and Phillips (1975), Hight et al. (1983), Miura et al. (1986), Pradel et al. (1990), Naughton and O'Kelly (2007), O'Kelly and Naughton (2009) and by Chairo et al. (2013). While these studies indicated some variation in the friction angle, none provided a complete picture.

4. Shear band orientations in isotropic soil

It does not appear to be possible to intentionally create isotropic deposits of granular materials, i.e. a laboratory method does not exist by which isotropic specimens of granular materials can be produced. In fact, deposits generated by dry pluviation always behave as cross-anisotropic materials, because the particle contact points favor the vertical direction, and the deposit is therefore stiffer and stronger in the vertical direction. However, just as friction angles from conventional, vertical specimens are calculated and employed in most analyses procedures with the assumption that the soil is isotropic, angles of dilation are calculated from the principal strains with the assumption that the soil behaves as an isotropic material. Thus, the intermediate principal strain does not enter into the calculation of the dilation angle and therefore does not affect its value.

True triaxial tests on sands show that as the value of b [$=(\sigma_2-\sigma_3)/(\sigma_1-\sigma_3)$] increases, the axial strain at failure decreases (Lade and Duncan, 1973, Wang and Lade, 2001, Abelev and Lade, 2003). The specimens with higher b-values develop shear bands in the hardening regime and this causes failure to occur. The beginning of the shear banding may be observed just before the sudden drop in stress ratio, as analyzed by Wang and Lade (2001). The volume change behavior shows increasing dilation with increasing b-values, and the dilation angles are calculated from the slopes of the volume change curves at failure according to the following expression:

$$\sin\psi = -\frac{\Delta\varepsilon_1+\Delta\varepsilon_3}{\Delta\varepsilon_1-\Delta\varepsilon_3} = \frac{\Delta\varepsilon_1+\Delta\varepsilon_3}{\Delta\varepsilon_1+\Delta\varepsilon_3-2\Delta\varepsilon_1} = \frac{\Delta\varepsilon_v}{\Delta\varepsilon_v-2\Delta\varepsilon_1} \tag{1a}$$

$$\sin\psi = \frac{\Delta\varepsilon_v/\Delta\varepsilon_1}{\Delta\varepsilon_v/\Delta\varepsilon_1-2} \tag{1b}$$

in which $\Delta\varepsilon_v/\Delta\varepsilon_1$ is the slope of the volume change curve at failure. The expression for the dilation angle in Eq. (1) was introduced by Hansen (1958) to capture the rate of dilation more accurately than could be done by the Mohr–Coulomb failure criterion with associated plastic flow. The intermediate principal stress, σ_2, plays no role in the Mohr–Coulomb failure criterion, and the consequent expression for the dilation angle assumes no strains in the σ_2-direction, i.e. $\Delta\varepsilon_2=0$.

The direction of shear bands relative to the direction of the major principal stress, α, observed in experiments may be compared to those from existing classical theories (Roscoe 1970; Arthur et al., 1977; Arthur and Dunstan, 1982):

$$\text{Coulomb}: \ \alpha_C = 45^\circ + (\varphi/2) \tag{2}$$

$$\text{Roscoe}: \ \alpha_R = 45^\circ + (\psi/2) \tag{3}$$

$$\text{Arthur}: \ \alpha_A = 45^\circ + (\varphi+\psi)/4 \tag{4}$$

in which φ and ψ are the friction angle and the dilation angle, respectively.

The bedding planes of pluviated sand are typically horizontal and perpendicular to the major principal stress, σ_1, or they are vertical and parallel to σ_1 in true triaxial tests. Thus, the effect of any direction of σ_1 between vertical and horizontal relative to the bedding planes is not often investigated. Besides, the deformations in specimens with inclined bedding planes result in imposed moments and stress conditions not accounted for in the specimens, thus making the test results questionable (Saada, 1970).

True triaxial tests most often indicate that the measured shear band inclinations are located between those predicted by the Coulomb and Arthur expressions (Arthur et al., 1977, Roscoe, 1970). Similar conclusions were reached by Arthur et al. (1977) and Arthur and Dunstan (1982), and theoretical analyses performed by Vardoulakis (1980) also support these experimental findings.

5. Torsion shear tests on hollow cylinder specimens

Torsion shear tests performed on hollow cylinder specimens represents the better way of investigating the effects of principal stress directions on the behavior of the soil, because in these tests the bedding planes remain horizontal and the principal stresses are rotated relative to the bedding planes. In addition, there are only minor effects of imposed non-uniform stress conditions if the specimen is sufficiently thin-walled and sufficiently tall (Lade, 1981). In these experiments the direction of the major principal stress may be changed relative to the cross-anisotropic deposit created by dry pluviation. This allows studying the direction of shear banding relative to the direction of the major principal stress in cross-anisotropic sand deposits. The strength results of such torsion shear test on dense, Fine Nevada sand were presented by Lade et al. (2013), and the observed directions of shear banding are presented and analyzed here.

5.1. Sand tested

All torsion shear tests were performed on Fine Nevada sand, which is composed of subangular to subrounded grains consisting mainly of quartz (98%). The properties of this sand are as follows: Mean diameter, $D_{50}=0.23$ mm; coefficient of uniformity, 2.08; coefficient of curvature, 1.05; specific gravity, 2.65; maximum void ratio, 0.771; and minimum void ratio, 0.507.

5.2. Preparation of hollow cylinder specimens

The boundaries of the hollow cylinder specimen consisted of custom molded inner and outer latex rubber membranes attached to stainless steel end rings. Hollow cylinder specimens with horizontal bedding planes were prepared using the pluviation and saturation techniques described by Lade et al. (2013). All specimens had inner and outer radii of 18.0 cm and 22.0 cm, respectively, and the wall thickness was therefore 2.0 cm. The height of the hollow cylinder was 40 cm. Fig. 1 shows a photograph of a newly constructed, untested hollow cylinder specimen.

Molds or forming jackets were used to hold the inner and outer latex rubber membranes while pluviating the sand. Two factors affect the void ratio when pouring the sand: The drop height and the rate of sand pluviation. In order to ensure the same void ratio for each specimen, the sand was poured into a funnel with a small tube inside the mouth of the funnel ensuring a constant flow rate of sand. It was determined empirically that a drop height of 35 cm at the employed flow rate would create the desired void ratio. As the sand was deposited, the funnel was carefully raised to ensure a drop height of 35 cm and even bedding planes in the assembled mold. A void ratio, $e=0.53$ was targeted for each specimen. This corresponds to a relative density of 91% for the Fine Nevada sand.

The base plate of the torsion shear apparatus was rigidly attached to a rotary table, which was driven by a gear motor with a constant rotation rate, and resistance provided by a piston protruding through the top plate. The hollow cylinder

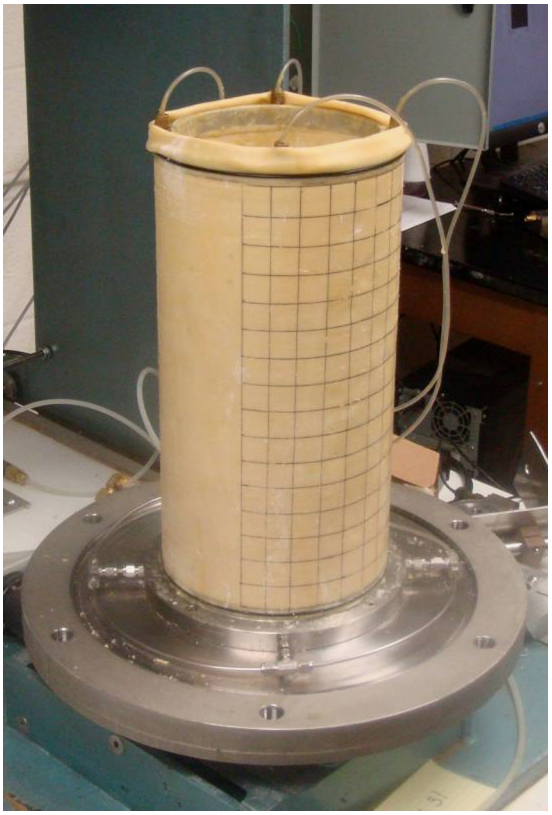

Fig. 1. Hollow cylinder specimen with grid. The torsion shear cell, with the specimen inside, sits on a rotary table, which is actuated by an electric motor.

specimen was sitting between a base ring and a top ring which in turn were attached to the base plate and the piston. Thus, the hollow cylinder specimen was exposed to the torque between the base plate and the piston. Separate pressures could be applied to the inner and outer cells in the new apparatus, making it possible to separate the principal stress inclination, α, from the value of $b=(\sigma_2-\sigma_3)/(\sigma_1-\sigma_3)$.

Measuring devices such as a vertical LVDT, horizontal LVDT, vertical load cell, torque arms and torque load cells were placed on the torsion shear apparatus prior to testing. Volume change devices were connected to the specimen and to the inner cell of the hollow cylinder.

A vertical LVDT was fastened to the piston to measure the axial deformations of the specimen. The shear deformation was measured at a constant distance from the center of the piston by a horizontal LVDT attached to the top plate of the chamber. A pie shaped plate with a groove along its curved edge was fixed to the piston. One end of the core of the horizontal LVDT was connected to the pie with an unstretchable radio cord. The radio wire cord was fastened to the core with a setscrew and ran along the groove of the pie.

A load cell was placed between the vertical piston and an air pressure cylinder located at the top of the rigid frame. To measure the shear stresses, a crossbar assembly was rigidly attached to the piston and two torque arms with load cells were connected to a back plate of the rigid frame.

The torque was used to calculate and control the vertical load and the inside and outside pressures in such a way as to follow a prescribed stress path. The pressures and forces in the torsion shear apparatus were computer controlled. The necessary equations were installed in the computer and for each prescribed increment in torque the vertical load and the inside and outside pressures were updated and applied. Since deformations were also measured, it was possible to calculate the actual pressures and shear stresses and apply them in real time. Further details regarding the specimen construction and saturation, the saturation of the inner cell, the instrumentation and the control of the experiments are given by Lade et al. (2013).

6. Experimental procedure and program

A series of 44 tests was performed in this experimental program to study the strength behavior and failure surface of Fine Nevada sand while keeping b, α and σ_m constant. A summary of the torsion shear tests is given in Table 1 where they are sorted by α-value and then b-value. Note that all friction angles have been adjusted to correspond to a common void of $e=0.53$. Skemptom's B-value was found and all specimens showed B-values above 0.94, which is acceptable for drained tests on dense sand. Prior to testing, the specimens underwent isotropic consolidation in increments in effective confining pressure of 6.9 kPa from 48.3 kPa to 101 kPa.

Shearing began for all specimens at the initial isotropic effective confining pressure of 101 kPa. Depending on the stress path indicated for the particular test, the vertical force was either in compression or extension, as indicated in Fig. 2 for constant mean stress, b-value and α-value. The inner and outer confining pressures either increased or decreased from the initial value of 101 kPa, as indicated in Fig. 3. The arrows show the direction of increasing difference in internal and external pressures for varying b-value and α-value. Every efforts was made to stay as close to the targeted b- and α-values as possible during testing.

To establish the failure conditions for all combinations of intermediate principal stress, as expressed by $b=(\sigma_2-\sigma_3)/(\sigma_1-\sigma_3)$, and σ_1-directions from $\alpha=0^\circ$ to $\alpha=90^\circ$, experiments were performed at each of the 25 intersection points of $b=0.0$, 0.25, 0.50, 0.75, and 1.00 and $\alpha=0^\circ$, 22.5°, 45.0°, 67.5°, and 90.0°. These experiments were performed while maintaining the mean normal stress constant at 101 kPa. For each of these experiments the stress–strain and volume change and strength behavior were determined.

Tests without principal stress rotation and with $\alpha=0^\circ$ and $\alpha=90^\circ$ do not require torque, and they are stress controlled tests. For these tests, the vertical load was applied in increments and the inner and outer cell pressures were changed accordingly to create different b-value conditions with a constant mean normal stress.

In some tests, corrections were applied to the data due to vertical piston uplift after the tests were performed, and the resulting α- and b-values were consequently not exactly the targeted values. However, since the stress path does not tend to affect failure, the failure points are presented for all tests. Following each experiment, the specimen was held on a

Table 1
Summary of torsion shear tests sorted by α-value and then b-value. Note that Void ratios are initial values and that friction angles have been adjusted to a common void ratio of $e=0.53$.

Test no.	Target α (°)	Actual α (°)	b-Value	Void ratio e	φ (°)	Test no.	Target α	Actual α	b-Value	Void ratio, e	φ (°)
23	0.0	0.0	0.00	0.531	41.2	12	45.0	47.9	0.80	0.559	40.3
1		0.0	0.00	0.510	36.8	13		48.2	0.96	0.553	39.3
24		0.0	0.27	0.530	45.8	34		45.0	1.00	0.541	35.6
25		0.0	0.55	0.530	53.1	14	67.5	67.3	0.00	0.538	35.1
2		0.0	0.75	0.529	56.9	35		65.1	0.16	0.531	37.6
26		0.0	1.00	0.532	53.3	36		67.8	0.25	0.533	37.6
3	22.5	22.4	0.00	0.523	39.3	15		67.5	0.50	0.525	39.5
27		24.0	0.02	0.510	36.3	37		65.0	0.55	0.528	38.1
28		23.7	0.23	0.531	43.4	38		65.1	0.75	0.528	31.8
4		23.7	0.27	0.548	47.3	39		64.4	0.79	0.531	34.8
5		23.5	0.27	0.524	41.4	40		61.9	0.80	0.541	34.9
6		22.5	0.50	0.526	43.4	16		71.5	0.96	0.536	29.2
29		22.2	0.75	0.531	46.6	17		68.2	1.00	0.532	38.3
30		22.9	0.85	0.529	46.2	41	90.0	90.0	0.00	0.523	33.2
7		24.5	0.89	0.552	43.1	18		90.0	0.04	0.530	33.9
8		22.5	0.99	0.541	42.9	19		90.0	0.07	0.538	38.2
31	45.0	44.9	0.02	0.535	36.2	42		90.0	0.32	0.530	45.0
32		31.6	0.18	0.560	40.2	20		90.0	0.54	0.530	45.2
9		45.0	0.25	0.530	38.9	43		90.0	0.78	0.520	39.2
33		45.0	0.50	0.528	45.0	21		90.0	0.78	0.520	40.4
10		47.4	0.54	0.555	39.9	22		90.0	0.99	0.520	36.7
11		45.0	0.75	0.540	40.4	44		90.0	0.99	0.510	36.7

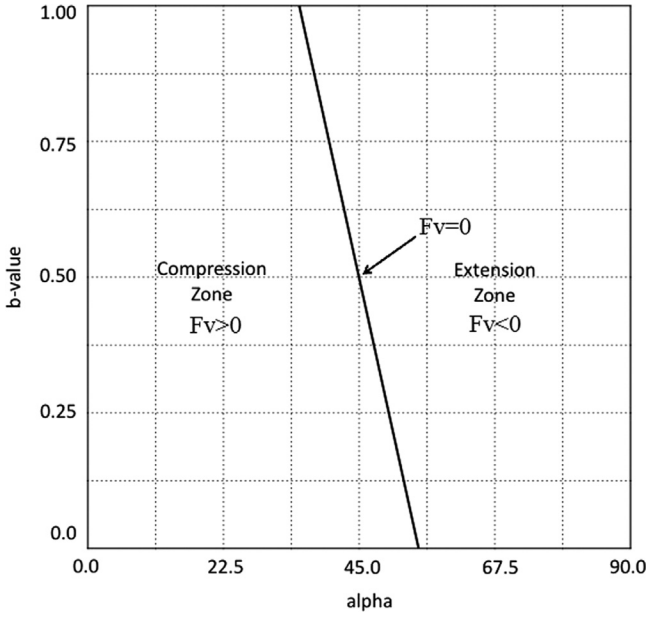

Fig. 2. Boundary area between compression and extension tests for torsion shear tests at constant values of α, b, and σ_m. Fv is the vertical compression/extension load in the central loading shaft.

vacuum for photographing and inspection for shear bands, the general shape and for taking final measurements.

7. Experimental results

As an example, the stress–strain and volume change behavior is shown in Fig. 4 for torsion shear tests with

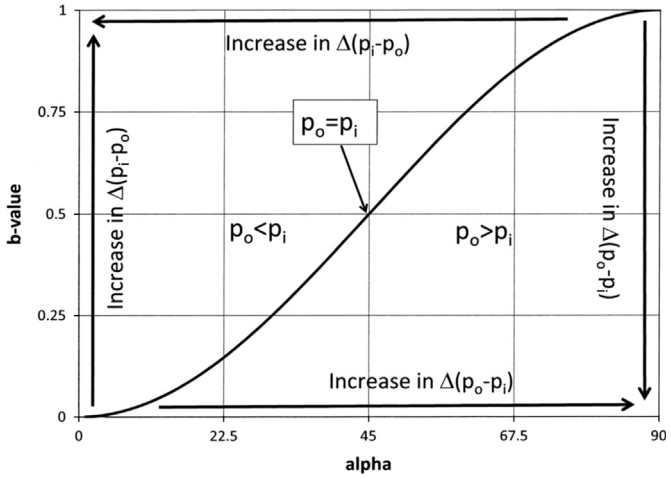

Fig. 3. Boundary area for inner and outer pressure conditions for torsion shear tests at constant values of α, b, and σ_m.

$\alpha=22.5^\circ$ and for all b-values from 0 to 1. The results are presented as stress ratio, σ_1/σ_3, versus the major principal strain, ε_1. These values are calculated from the measured normal and shear stresses and normal and shear strains. The results in Fig. 4(a) clearly indicate that the initial moduli increase, the strains-to-failure decrease, and the strengths increase with increasing b-value, except for $b=1$, where these quantities show the opposite behavior. The arrows indicate the points of failure. The volume change curves in Fig. 4(b) show that the rate of dilation increases with increasing b-values. The variation in behavior with b-values is very similar to that observed in true triaxial tests on sands (Lade and Duncan, 1973; Wang and Lade, 2001; Abelev and Lade, 2003).

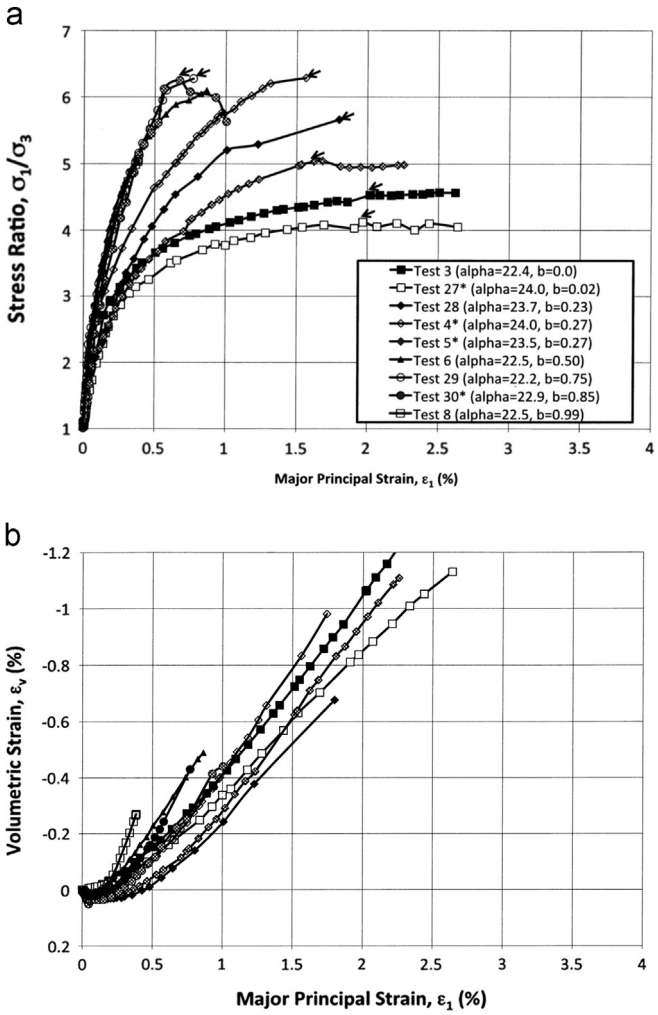

Fig. 4. (a) stress-strain and (b) volume change curves for torsions shear tests with $\alpha=22.5^{\circ}$.

The strength results of the torsion shear tests on Fine Nevada sand were presented and discussed by Lade et al. (2013). All friction angles obtained from the torsion shear tests have been corrected to correspond to the target void ratio of $e=0.53$ using the formula proposed by Caquot and Kerisel (1949): $e\cdot\tan\varphi=\text{const}$. Since the experiments were performed with the same mean normal stress and the friction angles are not sensitive to small variations in σ_m, it can be assumed that they correspond to the same value of $I_1=3\cdot\sigma_m=300$ kPa. Fig. 5 shows the three-dimensional variation in friction angle for $0\le b\le 1$ and for $0^{\circ}\le\alpha\le 90^{\circ}$. The surface presented in this diagram was modeled by a failure criterion for cross-anisotropic soils presented by Rodriguez and Lade (2013).

The angles of dilation, ψ, were determined for each experiment on the basis of the slope of the volume change relation at or near failure and calculated from Eq. (1). Fig. 6 shows the variation of ψ with b and α. This variation is the basis for the cross-anisotropic soil behavior. It was found that the angle of dilation was typically around 10° for most of the test conditions, and it was highest in the far corner ($\psi=28^{\circ}$) where $\alpha=0^{\circ}$ and $b=1.0$. It then varied in a smooth fashion with α and b. Just like the variation of the friction angle, the lowest values of the dilation angle were exhibited at an inclination of the major principal stress of $\alpha=67.5^{\circ}$, which corresponds approximately to sliding in the direction of least resistance.

8. Shear bands in cross-anisotropic sand

The shear band directions were measured at the end of each test while the specimen was held in a vacuum. The grid drawn on the surface of the specimen prior to shearing, shown in

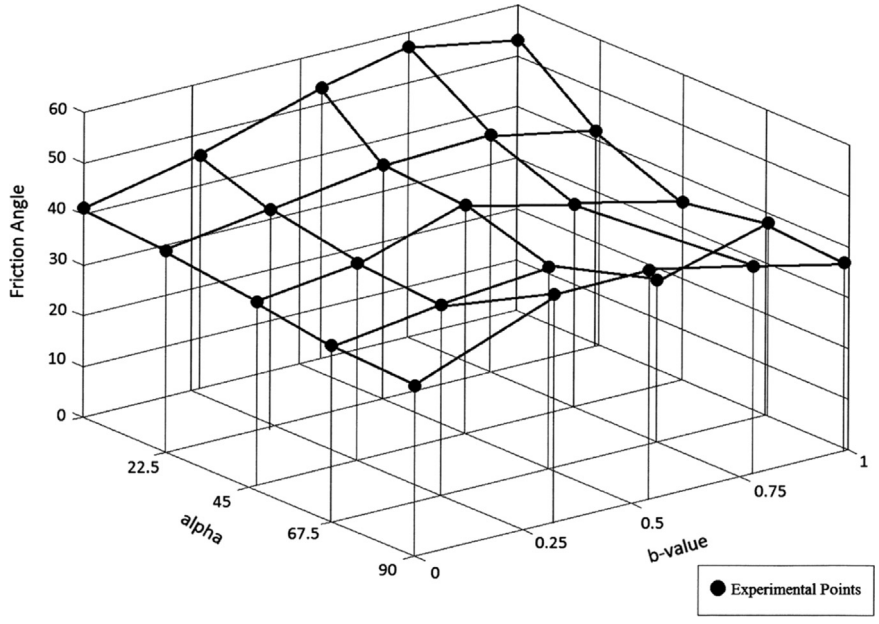

Fig. 5. Composite α-b-φ diagram of three-dimensional failure surface for dense Fine Nevada sand.

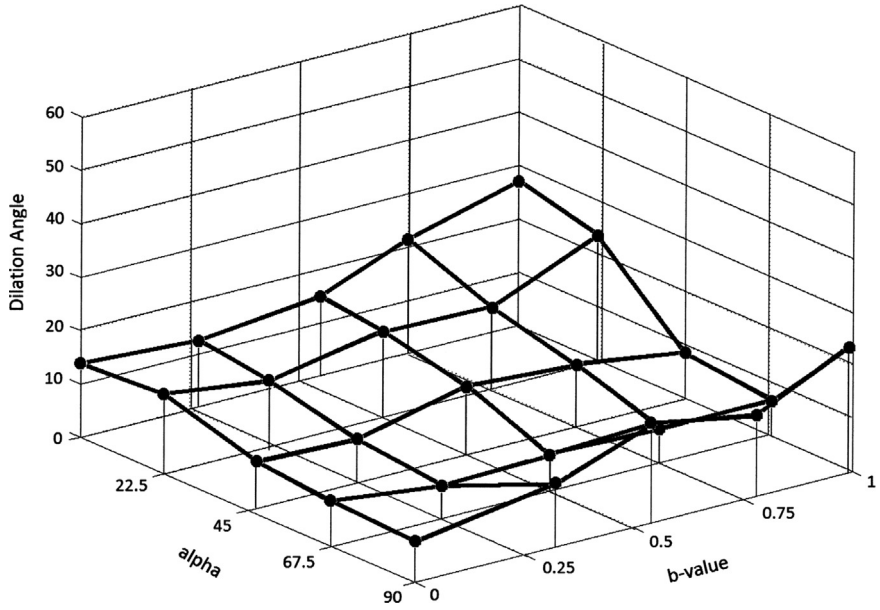

Fig. 6. Composite α-b-ψ diagram for cross-anisotropic deposits of dense Fine Nevada sand.

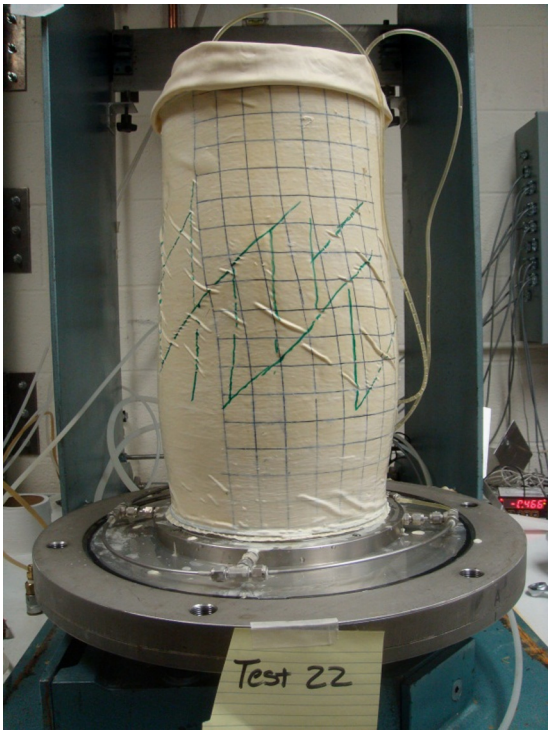

Fig. 7. Hollow cylinder specimen after failure under stress conditions with $b=0.25$ and inclination of major principal stress relative to vertical at $\alpha=22.5^{\circ}$.

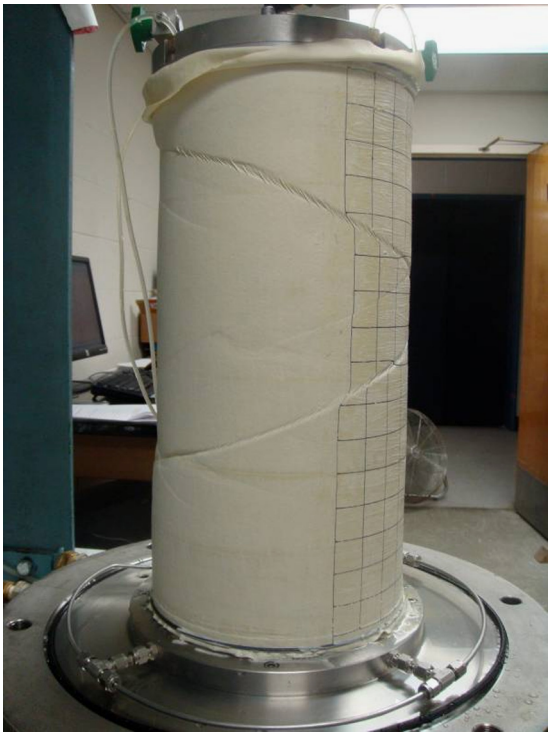

Fig. 8. Hollow cylinder specimen after failure under stress conditions with $b=0.25$ and inclination of major principal stress relative to vertical at $\alpha=90^{\circ}$.

Fig. 1, proved helpful in measuring the angles of the shear bands correctly. Usually, the shear bands are oriented such that the normal to the shear band is contained in the wall (Lade et al., 2008), as indicated on the photographs in Figs. 7–9. All but the experiments at b=0.0 resulted in peak failure caused by the development of shear bands. The experiments with b=0.0 exhibited smooth peak failure with shear banding developing in the softening regime.

Figs. 10–14 show comparisons of the measured shear band directions, β, relative to the σ_1-directions with the theoretical directions calculated from Eqs. (2)–(4) for all the torsion shear tests. The shear band inclinations typically vary within 5 to 10 degrees along its length around the hollow cylinder specimens due to small variations in void ratio. Such local variations in void ratio played a larger role in the hollow cylinder tests where the specimen volume was stretched out in a relatively thin wall, as may be characterized by a large surface area-to-

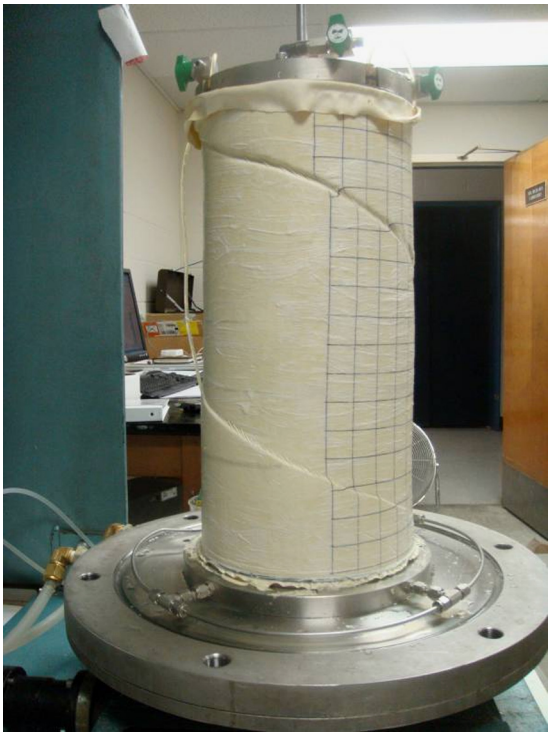

Fig. 9. Hollow cylinder specimen after failure under stress conditions with $b=0.59$ and inclination of major principal stress relative to vertical at $\alpha=90^\circ$.

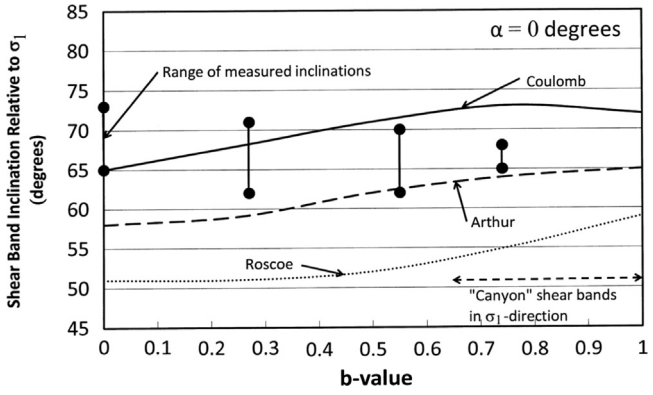

Fig. 10. Shear band inclination relative to σ_1-direction for torsion shear tests with $\alpha=0^\circ$.

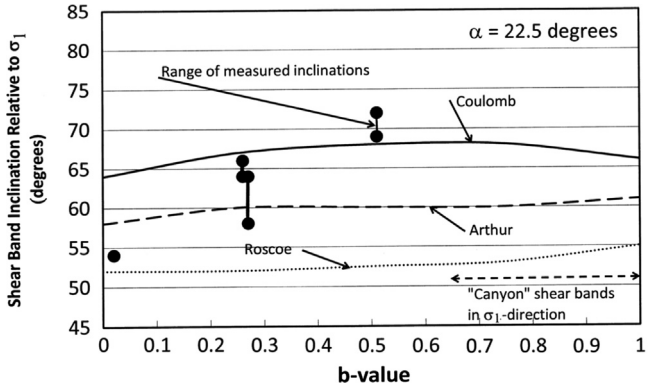

Fig. 11. Shear band inclination relative to σ_1-direction for torsion shear tests with $\alpha=22.5^\circ$.

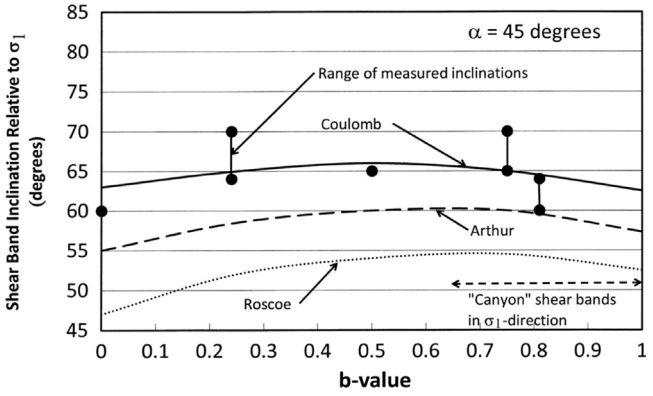

Fig. 12. Shear band inclination relative to σ_1-direction for torsion shear tests with $\alpha=45^\circ$.

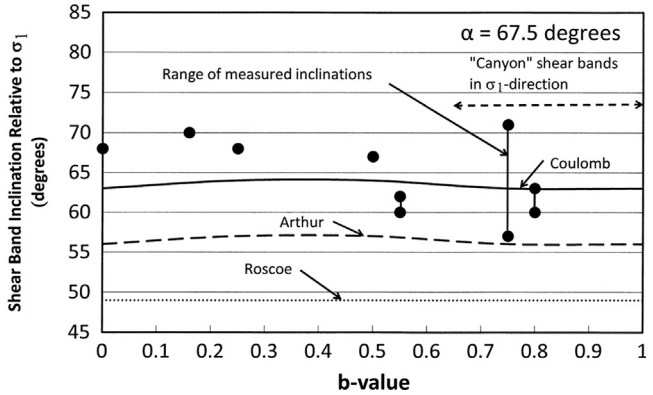

Fig. 13. Shear band inclination relative to σ_1-direction for torsion shear tests with $\alpha=67.5^\circ$.

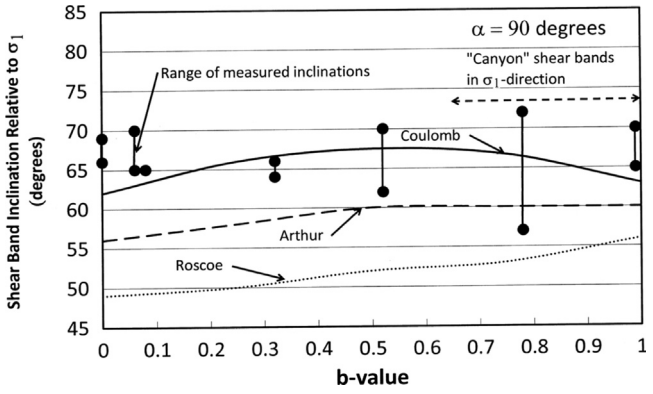

Fig. 14. Shear band inclination relative to σ_1-direction for torsion shear tests with $\alpha=90^\circ$.

volume (A/V), compared to other experiments, where the specimen volumes were more amassed, corresponding to smaller values of A/V. More consistent shear band directions were observed in the latter type of experiments. Thus, complete consistency between the experimental results and the theoretically predicted inclinations for the torsion shear tests could not be accurately predicted. The large β-ranges of 14° shown for α=67.5° and b=0.75 and 15° for α=90° and b=0.78 (in Figs. 13 and 14) each correspond to measurements

on two hollow cylinder specimens and thus includes the scatter from one to another specimen. Within this scatter, the diagrams in Figs. 10–14 show that the shear band inclination in the torsion shear tests appear to fit best with the variation proposed by the Coulomb direction, i.e. the shear bands tend to form angles of $\pm(45^\circ - \varphi/2)$ with the direction of the major principal stress, σ_1, or $\beta = \pm(45^\circ + \varphi/2)$ with the σ_1-plane, as shown in the diagrams. This is true for all α-angles and low to medium b-values with one exception to be discussed below. Examples are shown in Figs. 7–9.

For high b-values, the hollow cylinder specimens showed more than one type of shear band pattern. This is due to the cross-anisotropic character of the sand deposit for which the shear strength is lower in the horizontal direction than in the vertical direction. Thus, shear failure would occur in the horizontal direction and across the wall for high b-values, even though the intermediate principal stress, σ_2, was smaller than the major principal stress, σ_1. This has previously been observed in true triaxial tests on cross-anisotropic sand deposits (Abelev and Lade, 2003). For b-values greater than 0.6–0.7, horizontal shear failures were observed in all the hollow cylinder specimens, independent of the inclination, α, of the major principal stress. The cut-off value of b (0.6–0.7) for the occurrence of "canyon" shear bands depends on the degree of cross-anisotropy of the sand deposit. For these higher b-values, the Coulomb inclination of the shear bands were observed in all experiments, but additional shear banding occurred across the wall thickness of the specimen.

Fig. 15 shows two sketches of the shear band pattern for high b-values. In both cases the shear bands appear to be inclined in the σ_1-direction, but this is because extension type conditions occur with the minor principal stress perpendicular to the indicated σ_1-directions. The shear bands therefore appear as wide "canyons" on the outside surface of the hollow cylinder specimen rather than as relatively thin shear bands of the type shown in Figs. 7–9. The ε_1-strains shown in Fig. 4 for the three tests with high b-values are those calculated for homogeneous strains: they were not affected by the shear banding initiated later in the σ_2-direction. Calculation of the correct ε_2-strains in the area of the "canyon" is not possible (and they would not correspond to uniform strains), but once the shear banding initiates in the horizontal direction, the shear strength in the σ_1-direction is also affected and it begins to decline.

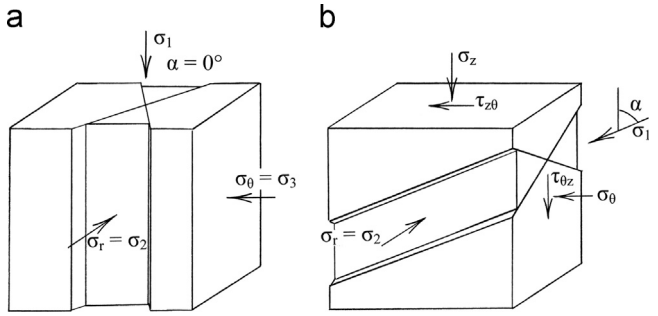

Fig. 15. Sketches of shear band pattern in torsion shear tests on cross-anisotropic sand deposits tested at high b-values.

Examples of shear banding at high b-values are shown in Figs. 16–20. The photos correspond to α-values close to 0°, 22.5°, 45°, 67.5° and 90°. The actual values of α and b at the

Fig. 16. Shear band pattern in hollow cylinder specimen with $\alpha = 0^\circ$ and $b = 0.79$. The outer layer of the membrane has been peeled off to clearly show the width and the sides of the "canyon" shear band oriented vertically in the direction of the major principal stress.

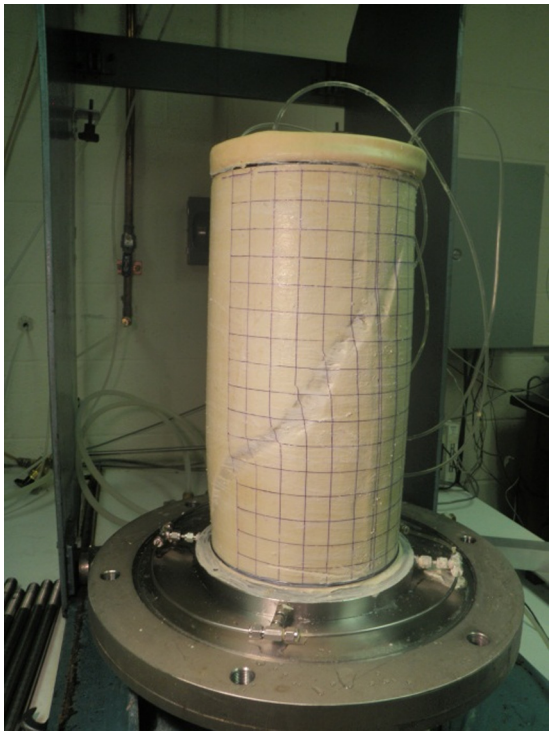

Fig. 17. "Canyon" shear band pattern in hollow cylinder specimen with $\alpha = 22.5^\circ$ and $b = 0.76$ oriented in direction of the major principal stress.

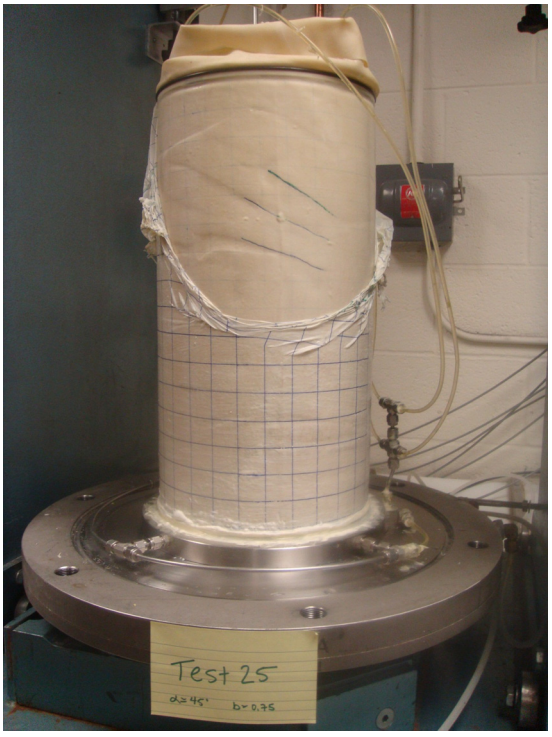

Fig. 18. Shear band pattern in hollow cylinder specimen with $\alpha=45^\circ$ and $b=0.75$. The outer layer of the membrane has been peeled off to clearly show the shear bands. Note the "canyon" shear bands across the width of the wall and the shear bands inclined at "conventional" directions, and the shear band under the steel cap ring.

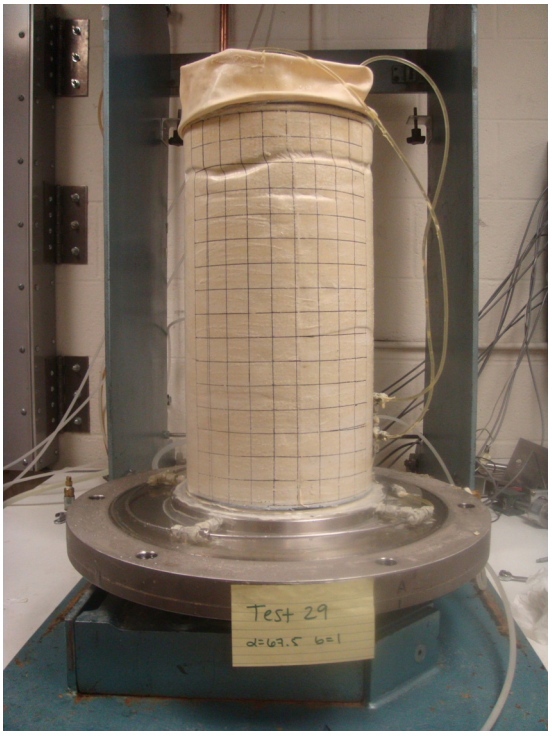

Fig. 19. Shear band pattern in hollow cylinder specimen with $\alpha=67.5^\circ$ and $b=1.0$. A combination of a "conventional" and a "canyon" shear band is observed.

Fig. 20. Shear band pattern in hollow cylinder specimen with $\alpha=90^\circ$ and $b=1.0$. The outer layer of the membrane has been peeled off to clearly show the shear bands. A combination of "conventional" and "canyon" shear bands are observed.

time of shear banding are given in the legends of the photos. It is clear that the reason these shear bands occur is that the surrounding flexible rubber membrane allows non-uniform deformations to occur. If the membranes had been rigid rather than flexible, then shear banding would have been impeded or prevented until higher stresses were reached. This was discussed by Lade and Wang (2012a, 2012b).

Note that the vertical "canyon" shear band in Fig. 16 occurs due to shear banding in the radial direction, but no shearing occurs along the shear band in the vertical direction due to the stiff steel end rings. Neither does shear banding occur at angles of $45^\circ \pm \varphi/2$ relative to vertical, because the configuration and kinematic constraints of the hollow cylinder specimen does not allow this to occur. For the remaining tests in Figs. 17–20, shearing along the "canyon" shear band created by the radial stress can occur because it is not inhibited by stiff ends. In the test in Fig. 20 with $\alpha=90^\circ$ and $b=1.0$, a combination of "conventional" and "canyon" shear bands are observed, because both patterns are equally likely.

For values of b near zero, the shear banding in cross-anisotropic sand with horizontal bedding planes should be equally likely in the σ_1–σ_3 plane and in the σ_1–σ_2 plane. However, the kinematic conditions and the different inside and outside pressures determine the modes of developing shear banding. Shear bands developed in the wall for $\alpha=0^\circ$ with a zigzag pattern around the hollow cylinder specimen. When $\alpha=22.5^\circ$, however, shear bands apparently developed simultaneously in both the σ_1–σ_3 plane and in the σ_1–σ_2 plane. This combined shear band was located both in the σ_1–σ_3 plane (in the wall) in a direction of 60° from vertical, as shown in Fig. 21(a), and it was observed as a bulge in the σ_1–σ_2 plane. The inclination angle in the σ_1–σ_3 plane is close to $\alpha+(45^\circ-\psi/2)$, i.e. the dilation angle appears to control the direction of the shear band in this experiment. This combined shear band is shown in the sketch in Fig. 21(b). For $b=0.0$ and $\alpha=67.5^\circ$ and 90° the outside pressure was higher than the inside pressure and for these cases the hollow cylinders imploded, as exemplified in Fig. 22.

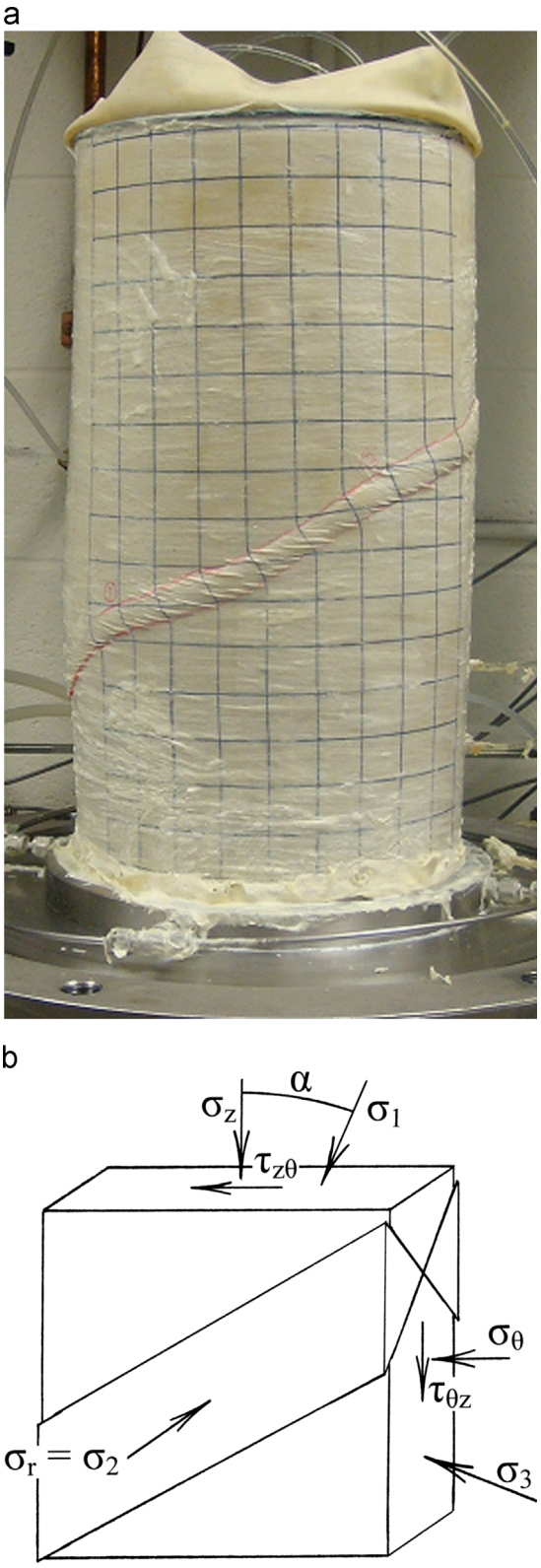

Fig. 21. (a) Shear band pattern in hollow cylinder specimen with $\alpha=22.5^\circ$ and $b=0.0$, and (b) Sketch of shear band pattern in torsion shear tests on cross-anisotropic sand deposit tested at $\alpha=22.5^\circ$ and $b=0.0$.

Thus, it appears that the loading scheme to create various conditions of α and b and the kinematic constraints in the torsion shear tests on hollow cylinder specimens impose certain limitations on the failure modes in the cross-anisotropic sand deposits and they are apparently affected by the boundary conditions provided in these tests.

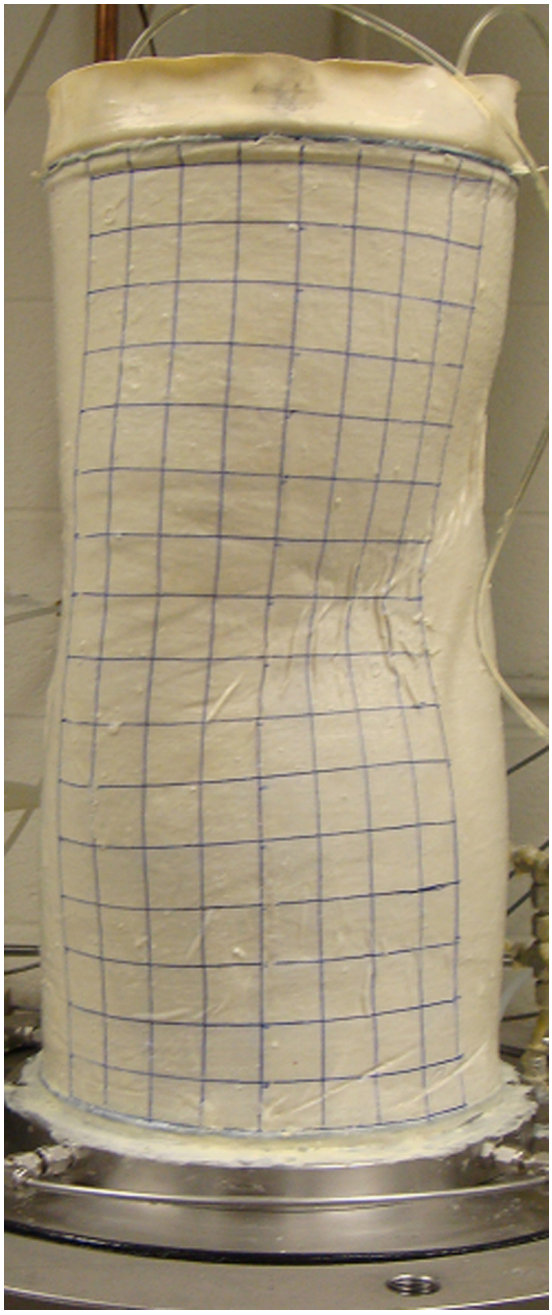

Fig. 22. Implosion of hollow cylinder specimen tested in torsion shear at $\alpha=90^\circ$ and $b=0.0$.

9. Effects of stiff and flexible boundaries

It is clear from the observed cross-anisotropic behavior in torsion shear tests and the explanations given above that the stiffness of the boundaries surrounding the specimen is important for experiments with high b-values in which failure can occur in the direction of the intermediate principal stress. This is partly because the strength is lower in the horizontal

directions than in the vertical direction, but additional effects are at play.

In triaxial extension tests ($b=1.0$) performed on cross-anisotropic sand specimens with stiff and flexible boundaries, Lade and Wang (2012a, 2012b) found that in specimens with stiff boundaries the specimens showed greater moduli, even at very small strains, lower strain-to-failure and greater strengths than in specimens with flexible boundaries. While the flexible membranes allow development of non-uniform strains, shear bands and necking, this is not sufficient to account for the large differences in strengths obtained from the two types of boundaries. In comparison, the stiff, smooth boundaries impose uniform strains at the boundaries. The behavior of the granular material inside the specimen may be affected by the movement of the individual grains in the specimen, which in turn is affected by the boundary conditions: Lade and Wang (2012a, 2012b) speculated that force chains may be supported and become stronger under enforced uniform strains, while they may be allowed to buckle under flexible boundary conditions, thus producing a weaker response to similar external stresses. Such different behavior has been observed in DEM calculations of assemblies of spherical grains, as presented by Tordesillas et al. (2008, 2011), Peters and Walizer (2013) and Cooper (2011). Whether this ultimately explains the observed behavior is unknown at this time.

It is interesting to speculate which type of behavior will prevail in the real ground, where boundary conditions are not imposed or controlled as in the laboratory experiments. It would seem most logical to argue that the soil behavior would be that corresponding to the flexible boundaries, unless the soil element in question is bordering a stiff boundary such as a steel or concrete surface. However, the flexible boundaries allow non-uniform strains to develop with consequent lower moduli, higher strain-to-failure and lower strengths than specimens with stiff boundaries. In experiments, even though the goal was to observe the soil behavior during uniform strains, this observed behavior may not be the most appropriate for real ground conditions, because of the differences resulting from flexible boundary conditions. This point requires further clarification after additional experimentation and discussion.

10. Conclusions

Experimental research is being performed to contribute to establishment of more realistic modeling of soil behavior. Many real soils, as they occur in-situ, clearly exhibit cross-anisotropic behavior with a vertical axis of rotational symmetry. This real behavior is most often assumed to be isotropic, and a number of observed behavior patterns are therefore not predicted correctly. Torsion shear experiments were performed on hollow cylinder specimens to determine the behavior and variation of the friction angle of dense, Fine Nevada sand deposited with cross-anisotropic fabric. Systematic variations in the intermediate princial stress and directions of the major principal stress were employed in these experiments. For a constant value of $b=(\sigma_2-\sigma_3)/(\sigma_1-\sigma_3)$, the friction angle was found to vary by 4° at $b=0.0$ to 16° at $b=0.75$ as the σ_1-direction changes from vertical to horizontal. However, for a given void ratio and all b- and α-values, the friction angle varied by as much as 22°. Based on these results and previous studies, it appears that six different factors play important roles in determining the friction angle for a given sand: (1) initial void ratio, (2) minor principal stress, (3) intermediate principal stress, (4) cross-anisotropic fabric, (5) orientation of the major principal stress relative to the bedding planes, and (6) occurrence of shear bands.

The effects of stiff and flexible boundaries on the behavior of the cross-anisotropic granular material is pronounced at high b-values, where shear banding can occur across the hollow cylinder wall because the strength is lower in the horizontal directions than in the vertical direction, but additional factors appear to be at play. Lade and Wang (2012a, 2012b) found that in true triaxial specimens with stiff boundaries the specimens showed greater moduli, even at very small strains, lower strain-to-failure and greater strengths than in specimens with flexible boundaries. These are likely to be present in the horizontal directions of the hollow cylinder specimens, where the flexible membranes allow non-uniform strains, early shear banding and lower strengths.

In view of the fact that endeavors have been made over the years to test soils under uniform strain conditions, which may be imposed by stiff, smooth boundaries, it is interesting to observe that the more likely conditions in the real ground are those corresponding to flexible boundary conditions in the laboratory. The latter boundary conditions may allow non-uniform strains to develop with consequent lower moduli, higher strain-to-failure and lower strengths than specimens with stiff boundaries. This raises many questions which require further clarification in view of additional experimentation and discussion.

Acknowledgements

The research presented here was performed with support from the National Science Foundation under Grant no. CMMI-0757827. Grateful appreciation is expressed for this support.

References

Abelev, A.V., Lade, P.V., 2003. Effects of cross-anisotropy on three dimensional behavior of sand. I: stress–strain behavior and shear banding. J. Eng. Mech., ASCE 129 (2), 160–166.

Abelev, A.V., Lade, P.V., 2004. Characterization of failure in cross-anisotropic soils. J. Eng. Mech., ASCE 130 (5), 599–606.

Arthur, J.R.F., Dunstan, T., 1982. Rupture layers in granular media. In: Vermeer, P.A., Luger, H.J. (Eds.), Proc. IUTAM Symposium on Deformation and Failure of Granular Media. Balkema, Rotterdam, The Netherlands, pp. 453–459.

Arthur, J.R.F., Menzies, B.K., 1972. Inherent Anisotropy in a Sand. Geotechnique 22 (1), 115–128.

Arthur, J.R.F., Phillips, A.B., 1975. Homogeneous and layered sand in triaxial compression. Geotechnique 25 (4), 799–815.

Arthur, J.R.F., Dunstan, T., Al-Ani, Q.A.J.L., Assadi, A., 1977. Plastic deformation and failure in granular media. Geotechnique 27 (1), 53–74.

Bishop, A.W., 1966. The strength of soils as engineering material, 6th Rankine Lecture. Geotechnique 16 (2), 89–130.

Caquot, A., Kerisel, J., 1949. Traite de Mechanique des Sols. Gauthier-Villars, Paris.
Chairo, G., Kiyota, T., Koseki, J., 2013. Strain localization characteristics of loose saturated Toyoura sand in undrained cyclic torsional shear tests with initial static shear. Soils Found. 53 (1), 23–34.
Cooper, W.L., 2011. Communication of stresses by chains of grains in high-speed particulate media impacts. SEM XI Int. Cong. Expos. Exp. Appl. Mech., 13–17 (Uncasville, CT, June).
Hansen, B., 1958. Line ruptures regarded as narrow rupture zones – basic equations based on kinematic considerations. Proceedings of the Conference on Earth Pressure Problems Vol. I, 39–48 (Brussels, Belgium).
Haruyama, M., 1981. Anisotropic deformation-strength characteristics of an assembly of spherical particles under three-dimensional stresses. Soils Found. 21 (4), 41–55.
Hight, D., Gens, A., Symes, M., 1983. The development of a new hollow cylinder apparatus for investigating the effects of principal stress rotation in soils. Geotechnique 33 (4), 355–383.
Lade, P.V., 1981. Torsion shear apparatus for soil testing. In: Yong, R.N., Townsend, F.C. (Eds.), Lab. Shear Strength Soil, ASTM STP 740. ASTM, pp. 145–163.
Lade, P.V., Abelev, A.V., 2003. Effects of cross-anisotropy on three-dimensional behavior of sand. Part II: volume change behavior and failure. J. Eng. Mech., ASCE 129 (2), 167–174.
Lade, P.V., Abelev, A.V., 2005. Characterization of cross-anisotropic soil deposits from isotropic compression tests. Soils Found. 45 (5), 89–102.
Lade, P.V., Duncan, J.M., 1973. Cubical triaxial tests on cohesionless soil. J. Soil Mech. Found. Div., ASCE 99 (SM10), 793–812.
Lade, P.V., Nam, J., Hong, W.P., 2008. Shear banding and cross-anisotropic behavior observed in laboratory sand tests with stress rotation. Can. Geotech. J. 45 (1), 74–84.
Lade, P.V., Rodriguez, N.M., Van Dyck, E.J., 2013. Effects of principal stress directions on 3d failure conditions in cross-anisotropic sand. J. Geotech. Geoenviron. Eng., ASCE 139, 12.
Lade, P.V., Wang, Q., 2012a. Method for uniform strain extension tests on sand. Geotech. Test. J. 35 (4), 607–617.
Lade, P.V., Wang, Q., 2012b. Effects of stiff and flexible boundary conditions in triaxial extension tests on cross-anisotropic sand behavior. Geotech. Test. J., ASTM 35 (5), 715–727.
Lade, P.V., Wasif, U., 1988. Effects of height-to-diameter ratio in triaxial specimens on the behavior of cross-anisotropic sand. Adv. Triaxial Test. Soil Rock, ASTM STP 977, ASTM, 706–714 (Philadelphia).
Lade, P.V., Yamamuro, J.A., 1996. Undrained sand behavior in axisymmetric tests at high pressures. J. Geotech. Eng., 122. ASCE120–129.
Lam, W.K., Tatsuoka, F., 1988. Triaxial compressive and extension strength of sand affected by strength anisotropy and sample slenderness.". Adv. Triaxial Test. Soil Rock, ASTM STP 977, ASTM, 655–666 (Philadelphia, PA).
Lee, K.L., Seed, H.B., 1967. Drained strength characteristics of sands. J. Soil Mech. Found. Div., ASCE 93 (SM6), 117–141.
Miura, K., Miura, S., Toki, S., 1986. Deformation behavior of anisotropic dense sand under principal stress axes rotation. Soils Found. 26 (1), 36–52.
Naughton, P.J., O'Kelly, B.C., 2007. Stress non-uniformity in a hollow cylinder torsional sand specimen. Geomech Geoeng. 2 (2), 117–122.
Ochiai, H., Lade, P.V., 1983. Three-dimensional behavior of sand with anisotropic fabric. J. Geotech. Eng., ASCE 109 (GT10), 1313–1328.
Oda, M., 1972a. Initial fabrics and their relations to mechanical properties of granular materials. Soils Found. 12 (1), 17–36.
Oda, M., 1972b. The mechanism of fabric changes during compressional deformation of sand. Soils Found. 12 (2), 1–18.
Oda, M., 1981. Anisotropic strength of cohesionless sands. J. Geotech. Eng. Div., ASCE 107 (GT9), 1219–1231.
Oda, M., Koishikawa, I., Higuchi, T., 1978. Experimental study of anisotropic shear strength of sand by plane strain test. Soils Found. 18 (1), 25–38.
O'Kelly, B., Naughton, P., 2009. Study of yielding of sand under generalized stress conditions using a versatile hollow cylinder torsional apparatus. Mech. Mater. 41 (3), 187–198.
Peters, J.F., Walizer, L.E., 2013. Patterned non-affine motion in granular media. J. Eng. Mech., ASCE 139 (10), 1479–1490.
Pradel, D., Ishihara, K., Gutierrez, M., 1990. Yielding and flow of sand under principal stress axes rotation. Soils Found. 30 (1), 87–99.
Rodriguez, N.M., Lade, P.V., 2013. Effects of principal stress directions and mean normal stress on failure criterion for cross-anisotropic sand. J. Eng. Mech., ASCE 139 (11), 1592–1601.
Roscoe, K.H., 1970. The influence of strains in soil mechanics. Geotechnique 20 (2), 129–170.
Rowe, P.W., 1962. The stress-dilatancy relation for static equilibrium of an assembly of particles in contact. Proc. Series A 269, 500–527 (R. Soc., Lond.).
Saada, A.S., 1970. Testing of anisotropic clay soils. J. Soil Mech. Found. Div., ASCE 96 (SM5), 1847–1852.
Tatsuoka, F., Sakamoto, M., Kawamura, T., Fukushima, S., 1986. Strength and deformation characteristics of sand in plane strain compression at extremely low pressures. Soils Found. 26 (1), 65–84.
Tordesillas, A., Multhuswamy, M., Walsh, S.D.C., 2008. Mesoscale measures of nonaffine deformation in dense granular assemblies. J. Eng. Mech., ASCE 134 (12), 1095–1113.
Tordesillas, A., Lin, Q., Zhang, J., Behringer, R.P., Shi, J., 2011. Structural stability and jamming of self-organized cluster conformations in dense granular materials,". J. Mech. Phys. Solids 59, 265–296.
Vardoulakis, I., 1980. Shear band inclination and shear modulus of sand in biaxial tests. Int. J. Numer. Anal. Methods Geomech. 4, 103–119.
Yamada, Y., Ishihara, K., 1979. Anisotropic deformation characteristics of sand under three dimensional stress conditions. Soils Found. 19 (2), 79–91.
Yamamuro, J.A., Lade, P.V., 1996. Drained sand behavior in axisymmetric tests at high pressures. J. Geotech. Eng., ASCE 122 (2), 109–119.
Wang, Q., Lade, P.V., 2001. Shear banding in true triaxial tests and its effect on failure in sand. J. Eng. Mech. ASCE 127 (8), 754–761.